ROYAL SOCIETY
OF CHEMISTRY

PAPER

Check for updates

Bio-gel derived nickel/carbon nanocomposites with enhanced microwave absorption†

Peitao Xie,‡[a] Hongyu Li,‡[a] Biao He,[a] Feng Dang,*[a] Jing Lin,*[b] Runhua Fan,*[c] Chuanxin Hou,[a] Hu Liu, [ID][de] Jiaoxia Zhang,[df] Yong Ma[dg] and Zhanhu Guo [ID] *[d]

A bio-gel derived strategy was used to construct Ni/C nanocomposites consisting of three-dimensional (3-D) carbon networks with embedded nickel nanoparticles. The amorphous carbon prevents agglomeration of the nickel nanoparticles and thus contributes to a good impedance match. The microwave absorption properties of the Ni/C nanocomposites were optimized according to percolation theory for good impedance matching. As a result, microwave absorbing coatings, which have the advantages of thin thickness (1.75 and 1.5 mm) and light weight (25 and 30 wt%), were achieved with excellent absorbing properties (90% microwave absorption) and a broad bandwidth (13.6–18 GHz and 13.2–18 GHz). The absorbing properties were mainly attributed to the dielectric relaxation processes at 2–18 GHz from the multilevel interface, porous carbon materials and nanoscale nickel nanoparticles in the Ni/C nanocomposites. It is believed that this work not only helps to elucidate the mechanism of absorption but also provides a new design paradigm for determining the optimal content of absorbers using percolation theory. The bio-gel derived strategy paves a possible way for the mass synthesis of microwave absorbers.

1. Introduction

The rapid development of wireless communications, normally operated in the GHz region, has led to severe electromagnetic (EM) pollution and radiation.[1–9] Normally, the methods used to solve these issues include absorption and reflection of the waves. However, only microwave absorption is efficient and can completely solve EM pollution because it can cut off the propagation of the EM waves, avoiding strong EM reflection and secondary pollution.[10–12] Hence, considerable efforts have been devoted to obtaining high-performance EM absorbing

materials with a high absorbing capacity and broad bandwidth. Generally, impedance matching and loss behaviors are the most important factors for absorbing EM waves.[13] Magnetic nickel has a large saturation magnetization value (55 emu g^{-1} at room temperature) and a high-frequency Snoek's limit (natural resonance can be as high as 8.23 GHz), allowing a high permeability in the GHz region to achieve good impedance matching, thus imparting it with the potential for excellent absorption.[14,15] However, when nickel matrix absorbing composites are put into a high-frequency EM field, the skin depth, especially for large metallic particles or agglomerated particles, decreases with increasing frequency, which prevents nickel from providing as good an impedance matching property as it theoretically can.[16–18]

Therefore, nickel nanostructures (such as wires, flakes, or hollow structures)[19–22] and composites (coatings or island-like structures) should be designed to obtain better impedance matching and to allow integration of more magnetic/dielectric absorption components.[23–26] Among these strategies, nickel/carbon (Ni/C) nanocomposites have the advantages of good impedance matching, strong dielectric loss and low density.[3,25–30] For example, porous Ni/C microspheres were fabricated via a solvothermal method combined with carbon reduction and their epoxy resin composites, containing 60 and 75 wt% porous Ni/C microspheres, showed an EM wave absorption of −10 dB at thicknesses of 3.0–11.0 and 1.6–7.0 mm.[25] The Ni/C core–shell nanoparticles were derived from metal–organic-frameworks (MOFs) and their paraffin composites, containing 40 wt% Ni/C

[a] *Key Laboratory for Liquid-Solid Structural Evolution and Processing of Materials (Ministry of Education), Shandong University, Jinan 250061, China. E-mail: dangfeng@sdu.edu.cn*

[b] *School of Chemistry and Chemical Engineering, Guangzhou University, Guangzhou 510006, China. E-mail: linjing@gzhu.edu.cn*

[c] *College of Ocean Science and Engineering, Shanghai Maritime University, Shanghai 201306, China. E-mail: rhfan@shmtu.edu.cn*

[d] *Integrated Composites Laboratory (ICL), Department of Chemical & Biomolecular Engineering, University of Tennessee, Knoxville, TN 37996, USA. E-mail: zguo10@utk.edu*

[e] *National Engineering Research Center for Advanced Polymer Processing Technology, Zhengzhou University, Zhengzhou 450002, China*

[f] *School of Material Science and Engineering, Jiangsu University of Science and Technology, Zhenjiang, Jiangsu, 212003, China*

[g] *College of Materials Science and Engineering, Shandong University of Science and Technology, Qingdao 266590, China*

† Electronic supplementary information (ESI) available. See DOI: 10.1039/c8tc02127a

‡ Peitao Xie and Hongyu Li contributed equally to this work.

nanoparticles, showed an EM absorption of −51.8 dB with a 2.6 mm thickness.[26] Carbon-coated nickel nanocapsules were prepared *via* an arc plasma reaction and their silicone nano-composites, containing 50 wt% Ni/C content, exhibited a maximum reflection loss (RL) value of −32 dB at a 2.5 mm thickness.[27] Thus, a high absorbing property could be easily achieved with a RL value of ∼−20 to −40 dB at different thicknesses in the composites with designed multilevel structures.[28–39] In fact, further reduction of the coating thickness is essential to their application, and decreasing the Ni/C content is also an important issue for realizing a light-weight absorbing coating under the premise of a lack of deterioration of the EM wave absorbing properties. Moreover, when Ni/C absorbers are used in practical applications, a high fabrication yield of the Ni/C absorber should be considered since this suppresses the development of some synthetic strategies for nano absorbers due to their low yields. Hence, some substitute solutions should be explored for the synthesis of Ni/C absorbers.

Biomineralization is an organic–inorganic hybrid process in which small crystalline units grow in the organic matrix to form a functional structure, such as seashells, teeth and bones. The microstructures are composed of uniformly organized primary particles from the nano to micrometer scale, resulting in unique architectures which can exhibit multifunctional properties.[40–42] This bio-gel derived strategy is usually used to fabricate inorganic powders or metallic/inorganic composites as anode materials for lithium-ion batteries. However, biomineralization is rarely applied for the preparation of carbon/metal composites, especially for the fabrication of microwave absorbers.

In this research, a bio-gel derived strategy was used to fabricate Ni/C nanocomposites in which Ni nanoparticles were uniformly distributed in a 3D carbon network. The microstructure and composition were analyzed using field emission scanning electron microscopy (FESEM), X-ray diffraction (XRD), Raman spectroscopy, X-ray photoelectron spectroscopy (XPS) and Fourier transform infrared (FT-IR) spectroscopy. The magnetization loop at room temperature was evaluated using a vibrating sample magnetometer. The electromagnetic properties were tested using a network-analyzer. The presence of a carbon network is greatly beneficial to prevent the agglomeration of nickel particles and suppress the leakage current in the cross-linked nickel network. The optimized filler (Ni/C) content in the absorbing coatings was chosen using percolation theory to achieve good impedance matching properties. There are four different regions of dielectric response at 2–18 GHz in the absorbing composites due to their porous structure and multilevel interface, which contribute to the dielectric loss mechanism to achieve good EM absorbing properties. On the other hand, the magnetic properties of nickel nanoparticles partially offset the high-frequency diamagnetism of the carbon network, which is beneficial for matching between the dielectric properties and magnetic loss. High-performance EM absorbing materials were achieved *via* a bio-gel derived strategy with advantages such as light weight (25 wt% filler content), thin thickness (1.5 mm) and large-scale fabrication. The enhanced EM absorbing performances are explained in terms of dielectric relaxation loss of the multilevel carbon structure and ferromagnetic resonance of the nickel nano-particles together with other factors including eddy current loss.

2. Experimental

2.1. Chemicals

Nickel chloride ($NiCl_2 \cdot 6H_2O$) and ammonium hydrogen carbonate (NH_4HCO_3) were purchased from Sinopharm Chemical Reagent Co. Ltd China. The agar was purchased from Aladdin Reagent Co. Ltd. The chemicals were obtained as chemically pure grade products and used without any further treatment.

2.2. Biomimetic preparation of nickel/carbon nanoparticles

Precursor solutions were prepared by adding 12 g agar powder into 200 mL aqueous solution containing 0.15 mol $NiCl_2 \cdot 6H_2O$ with heating at 100 °C for 30 min. The precursor solutions were cooled and solidified at room temperature for 2 h, and then 200 mL 1.2 moL L^{-1} NH_4HCO_3 aqueous solution was poured onto the solidified precursor gel. The vessel was sealed for 48 h at room temperature. Nanoparticles of $NiCO_3$ formed with the infiltration of NH_4HCO_3 into the gel, and the $NiCO_3$ nano-particles were uniformly embedded and isolated in the agar gel. The obtained gel precursors were cut into pieces and they were then dried *via* a freeze-drying process in order to maintain the homogeneous morphology of the gel precursor. Nickel/carbon nanoparticles were produced by heating these powders at 600 °C for 6 h under an Ar atmosphere.

2.3. Characterization and measurement

The microstructure of the composites was studied using a field emission scanning electron microscope (FESEM, Hitachi SU-70, Tokyo, Japan) with electron energy dispersion spectroscopy (EDS). The phase identifications were investigated at room temperature from X-ray diffraction (XRD; Tokyo, Japan) using the Rigaku D/max-rB X-ray with Cu Kα radiation. Raman spectra were collected using a micro-Raman spectrometer (Jobin Yvon HR800, France) with 532.05 nm incident radiation. The Fourier transform infrared (FT-IR) spectra of the Ni/C nano-composites were obtained in the range of 500 to 4000 cm^{-1} using FT-IR spectroscopy (Bruker Inc. Vector 22, coupled with an attenuated total reflection accessory). The magnetization hysteresis loop of the Ni/C nanocomposites at room temperature was evaluated using a vibrating sample magnetometer (Tamakawa TM-VSM2014-MHR). Moreover, the Ni/C powders were homogeneously dispersed in paraffin at different mass ratios and then pressed into a toroidally-shaped sample (inner diameter 3.01 mm, outer diameter 6.99 mm) for measurement of the electromagnetic properties. The relative complex permittivity ($\varepsilon_r = \varepsilon_r' - j\varepsilon_r''$) and permeability ($\mu_r = \mu_r' - j\mu_r''$) of the Ni/C-paraffin composite materials were measured using the transmission/reflection method using a coaxial line cell and a network-analyzer (Agilent E5071C) in the frequency range from 10 MHz to 10 GHz. The RL results were calculated from μ_r, ε_r and absorber thickness using eqn (1) and (2):[43–45]

$$Z_{in} = Z_0(\mu_r/\varepsilon_r)^{1/2} \tanh[j(2\pi f d/c)(\mu_r \varepsilon_r)^{1/2}] \qquad (1)$$

$$RL = 20 \log|(Z_{in} - Z_0)|/|Z_{in} + Z_0| \qquad (2)$$

where f is the frequency of the electromagnetic field, d is the absorber thickness, c is the light velocity and Z_{in} and Z_0

represent the frequency input impedance and free-space impedance, respectively.

3. Results and discussion

The preparation process is illustrated in Fig. 1. In the preparation process, a homogeneous dispersion of Ni^{2+} in aqueous solution could be maintained after the precursor solutions were solidified. That is, a uniform dispersion of Ni^{2+} at a molecular level could be achieved in the gel. Then $NiCO_3$ formed with the infiltration of HCO_3^- into the gel, so the $NiCO_3$ nanoparticles were uniformly dispersed in the agar gel.[40–42] The agar network could be maintained *via* freeze-drying and transformed into a carbon network with a porous structure after pyrolysis. In addition, the $NiCO_3$ nanoparticles were reduced into nickel by the pyrolytic carbon.[3,38]

Fig. 2 shows SEM images of the Ni/C nanocomposites. The inset in Fig. 2a shows a direct image of the powder of the Ni/C nanocomposites produced in one experiment. It should be noted that the product yield can be scaled up to the kilogram scale by multiplying the reactant amount without changing the reaction temperature and time in this process, which enables this bio-inspired process to be utilized for practical applications. As shown in Fig. 2a, the Ni/C nanocomposites exhibit a sheet-like morphology with a size of over 20 μm and a thickness of *ca.* 1.5 μm. The carbon matrix exhibits a porous structure, and the Ni particles exhibit an irregular morphology and a size ranging from 100–500 nm and they are uniformly embedded in the carbon matrix (Fig. 2b–d). It is worth noting that the average size of the Ni particles on the surface of the carbon matrix (Fig. 2b and c) is obviously larger than the size of those embedded in the carbon matrix (Fig. 2d). It can be concluded that the porous carbon network could suppress the growth of the embedded nickel particles, but has little restriction effect on the growth of the Ni particles on the surface.[29,38,42] The surface of the carbon sheets is partly damaged due to the reduction of $NiCO_3$ (Fig. 2b). The uniformly distributed Ni particles in the carbon matrix are favourable for suppressing the leakage current across the whole composite to obtain better impedance matching and enhanced electromagnetic properties.

The XRD pattern of the Ni/C nanocomposites is shown in Fig. 3a. The three diffraction peaks at around 44.5°, 51.8° and 76.4° are indexed as face-centered cubic (fcc) nickel, which is in
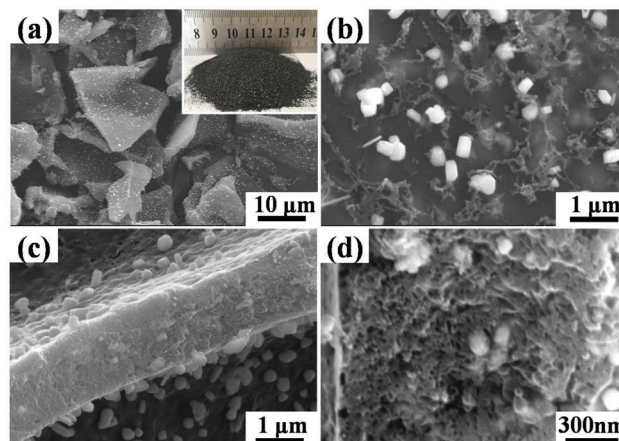

Fig. 2 SEM images of the Ni/C nanocomposites. (a) Low-magnification images, (b) the surface of the sheets, (c) the fracture surface of the sheets and (d) high-magnification images of the fracture surface of the sheets. The inset of (a) shows the experimental yield of the Ni/C nanocomposites produced in one experiment *via* a bio-gel strategy.

good agreement with JCPDS card 04-0850. The strong diffraction peaks indicate good crystallinity of the Ni particles. However, the diffraction peak of carbon cannot be clearly identified except for a weak peak at around 26°, indicating that the carbon is amorphous.[46–51] The Raman spectrum of the Ni/C nanocomposites is presented to aid in the investigation of the carbon materials (Fig. 3b). There are two broad overlapping peaks at around 1353 and 1572 cm^{-1}. The peak at 1572 cm^{-1}, known as the G band, originates from the in-plane vibration of the sp^2 carbon atoms, while the peak at around 1353 cm^{-1} is the D band, corresponding to the disordered structure of amorphous carbon.[46] The relative intensity of the D band and the G band (I_D/I_G) is used to evaluate the graphitic degree in carbon materials, *i.e.* the Tuinstra–Koenig (TK) equation. The intensity ratio (I_D/I_G) is about 1, and this value falls into the range of a structure transformation from nanocrystalline graphite to amorphous carbon, indicating that the carbon is amorphous.[52–56] The Raman results are in good agreement with the XRD analysis, evaluated from Fig. 3a.

The IR spectrum of the Ni/C nanocomposites was evaluated to further investigate the composition and chemical bonds of the composites and it is shown in Fig. 4a. There is no obvious absorption peak corresponding to the C–H groups.[57] The peaks at 3440, 1635 and 1098 cm^{-1} correspond to the adsorption of
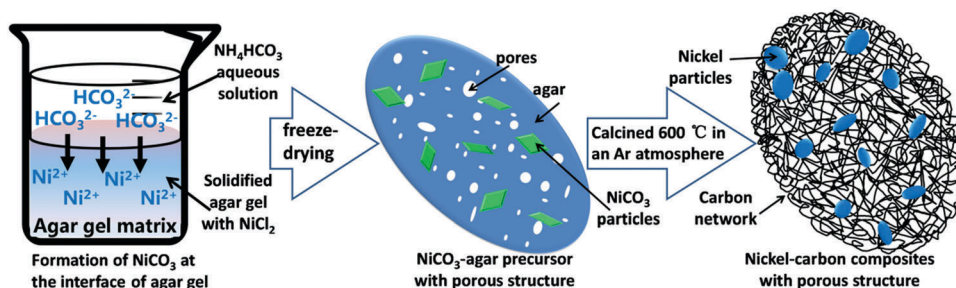

Fig. 1 Illustration of the preparation of the Ni/C nanocomposites *via* a bio-gel derived strategy.
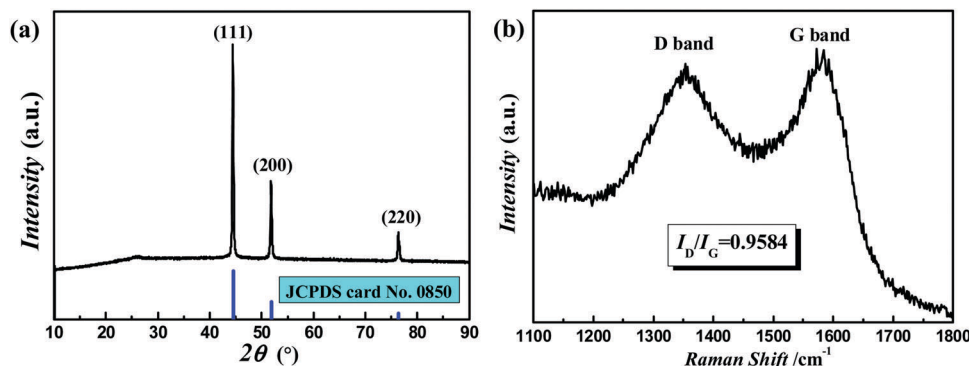
Fig. 3   XRD pattern (a) and Raman spectrum (b) of the Ni/C nanocomposites.

the O–H and C–O groups,[25,57–59] which indicates the incomplete pyrolysis of agar. The more detailed carbon structure was characterized using XPS. The deconvolution C_{1s} spectra are presented in Fig. 4b. The three peaks in the C_{1s} XPS spectra, C=C, C–C and C–O–C, correspond to the binding energies of 284.57 eV, 284.96 eV and 286.61 eV and they contribute ∼53.64%, 28.55%, and 17.81% to the total integrated intensity, respectively.[60–64] The XPS results indicate the existence of a large number of residual oxygen-containing groups, which is in agreement with the results from the IR spectrum. These oxygen-containing groups could interact with the electromagnetic waves for efficient enhancement of the microwave absorption properties.[65]

The pore distribution in the Ni/C nanocomposites was tested using the N_2 adsorption/desorption technique, as shown in Fig. 5. Three adsorption peaks can be observed, which correspond to pores with sizes of 1 nm, 10 nm and 100 nm. The highest adsorption peak corresponds to a 100 nm pore diameter, indicating that there are many macropores in the Ni/C nanocomposites. The micron-sized pores should be mainly related to the carbon matrix, as revealed in Fig. 2d, while the macropores are attributed to the damage due to the reduction of $NiCO_3$ (Fig. 2b). According to the IUPAC classification, all of the isotherms are a combination of type I and type IV isotherms corresponding to the micro-mesoporous materials.[66] As shown in Fig. 5b, the isotherms show higher adsorption at

high relative pressures, also indicating that the samples contain many macropores.[67]

Nine paraffin composites were prepared with different Ni/C contents, and their electromagnetic properties are shown in Fig. 6 and Fig. S1 (ESI†). The excellent absorbing materials should firstly exhibit good impedance matching properties to allow the EM waves to enter into the materials, and finally a high dielectric loss allows the EM waves inside the materials to be absorbed completely. This requires the paraffin composites to have an appropriate Ni/C content. In fact, the composites containing 25 and 30 wt% Ni/C had excellent absorbing properties which will be introduced in the following sections, while the other seven composites showed poor absorbing properties, as shown in Fig. S2–S4 (ESI†). Therefore, the content of Ni/C is the key factor in achieving excellent absorption properties, and the optimal content of the absorbing powders is determined to exhibit good impedance matching by percolation theory.

As shown in Fig. 6a, the real permittivity (ε') increases with increasing Ni/C content because of the enhanced interfacial polarization. With increasing the Ni/C content, polarization is enhanced not only due to the increased interface between Ni/C and paraffin but also due to the strong interface polarization inside the Ni/C powders. These interfaces can serve as microcapacitors. Therefore, the composites can be regarded as a network of microcapacitors, which can hold a large capacity to store electric charge, enabling the composites to possess a
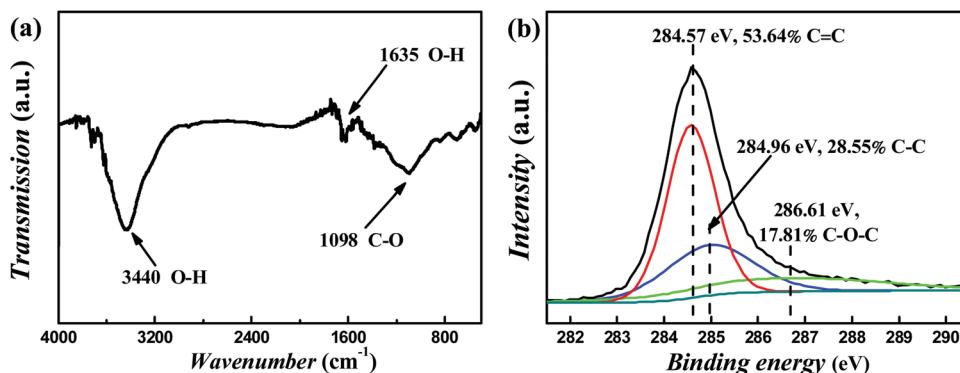

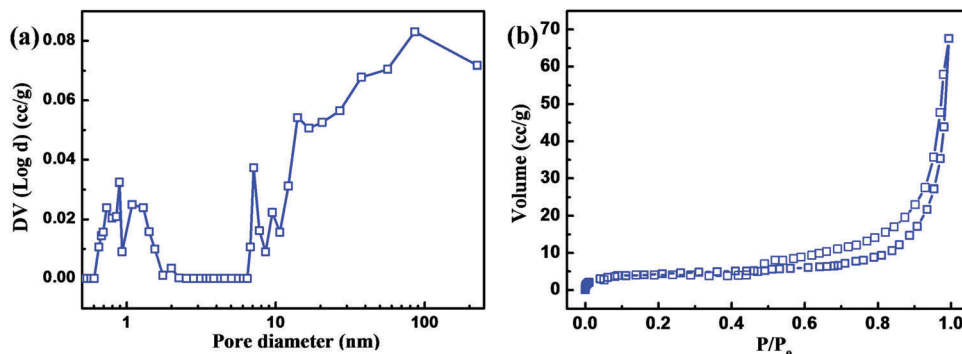Fig. 4   IR spectrum (a) and C_{1s} XPS spectra (b) of the Ni/C nanocomposites.

This journal is © The Royal Society of Chemistry 2018

J. Mater. Chem. C, 2018, 6, 8812–8822 | 8815

Fig. 5 Pore-size distribution (a) and nitrogen adsorption–desorption isotherm (b) of the Ni/C nanocomposites.
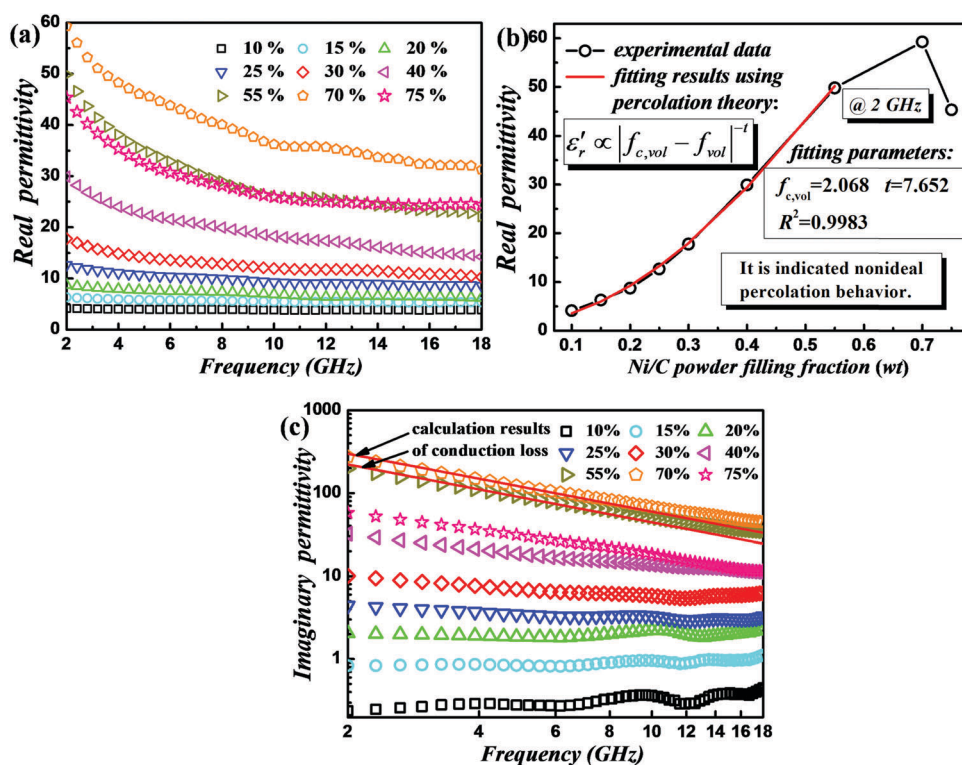

Fig. 6 The real permittivity (ε_r') of the paraffin composites containing different contents of Ni/C powder (a), the real permittivity (measured at 2 GHz) as a function of the mass fraction of the Ni/C powders in the paraffin composites (b) and the imaginary permittivity (ε_r'') spectra of the paraffin composites containing different Ni/C contents (c). The red solid lines in (b) are the fitting results obtained using percolation theory. The red solid lines in (c) are the calculation results obtained using the conduction loss.

high permittivity.[68] This mechanism is common in many dielectric composites and is also known as the Maxwell–Wagner–Sillars effect.[69–72] The Maxwell–Wagner–Sillars effect is enhanced when increasing the absorber content. In this work, the absorber is Ni/C powder, which can be somehow regarded as a conductor. Therefore, the paraffin composites can be seen as percolating composites. In fact, typical percolating composites consist of a conductive filler and an insulating matrix, and the relationship between real permittivity and filler content can be investigated using percolation theory:[73]

$$\varepsilon_r' \propto |f_{c,vol} - f_{vol}|^{-t} \qquad (3)$$

where $f_{c,vol}$ is the percolation threshold, f_{vol} is the volume fraction of the Ni/C powder and t is the dielectric critical exponent. Usually, percolation theory is used to describe the conductor–insulator transition in percolating composites when increasing the filler content. The percolation threshold is the critical filler content where the conductivity or real permittivity abruptly increases, indicating the formation of a conductive network in the composites and the transition from an insulator to a conductor.[60–62] As we know, we would like the absorber content to be as high as possible in order to achieve high absorption properties in the paraffin composites. On the other hand, too high an absorber content can also lead to reflection

8816 | *J. Mater. Chem. C*, 2018, **6**, 8812–8822

This journal is © The Royal Society of Chemistry 2018

of the microwaves, since it is well known that a conductor would result in strong reflection of electromagnetic waves.[6–9] Therefore, there is an optimal absorber content in the paraffin composites, where the best absorption properties can be observed, and this optimal content can be identified using percolation theory. As shown in Fig. 6b, the ε' increases rapidly with increasing Ni/C content in the 0.1–0.6 region and then decreases at high contents, which is typical percolating behavior.[69,73] The ε' was simulated using eqn (3) and the calculation results are represented as red solid lines in Fig. 6b. The obtained calculation parameters are $f_c = 2.068$ and $t = 7.652$ with a high reliability factor of $R^2 = 0.9983$. However, the parameters should always be $0 < f_c < 1$ and $t \approx 1$ in an ideal percolation model.[73,74] In typical percolation theory, the electrical percolating behavior is usually investigated and is significant in the low frequency region (direct current or kHz region) with the formation of a percolating conductive network. Besides, typical percolating composites are usually binary composites consisting of a conductor as the filler and an insulator as the matrix.[69–74] Therefore, the large calculation deviations from the ideal percolation theory are mainly attributed to the high-frequency region, the low conductivity of porous amorphous carbon and the multilevel structure in the Ni/C powders. However, it can be observed from Fig. 6b that the real permittivity increases obviously in the 0.3–0.55 region, so we can preliminarily conclude that the optimal absorber content is below 0.4, which is consistent with the experimental absorption properties (Fig. 7 and Fig. S2–S4, ESI†).

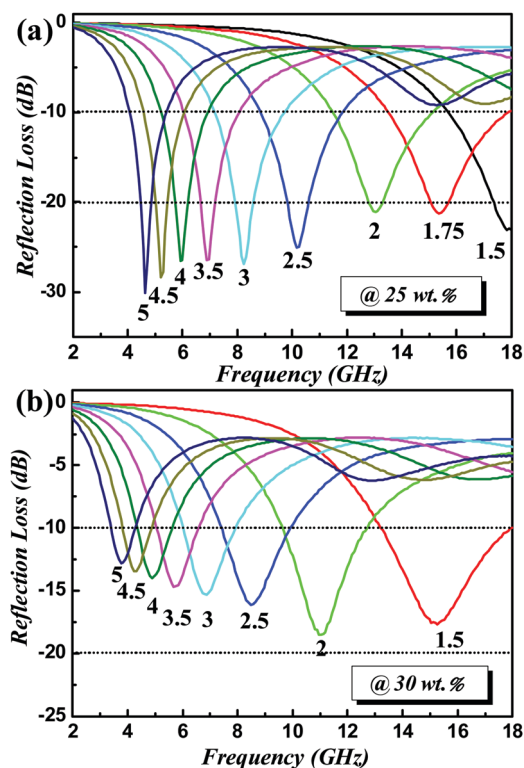In addition, the dielectric loss mechanism is different for composites below or above the percolation threshold, so we can also determine whether the absorber content exceeds the percolation threshold by analyzing the imaginary permittivity spectra. Fig. 6c shows the imaginary permittivity (ε'') spectra of the paraffin composites containing different Ni/C contents. The ε'' increases with increasing Ni/C content. ε'' suggests energy loss deriving from the leakage current and dipoles. That is, conduction loss and polarization loss. The conduction loss is not only determined by the carrier concentration and mobility but also the microstructure of the material, while the polarization loss is mainly attributed to the relaxation behavior of the dipoles in this frequency region. ε'' is expressed from a combined contribution of conduction and relaxation as follows:[75]

$$\varepsilon_r{}'' = \varepsilon_c{}'' + \varepsilon_p{}'' = \frac{\sigma}{\omega\varepsilon_0} + \frac{\varepsilon_s - \varepsilon_\infty}{1 + \omega^2\tau^2}\omega\tau \qquad (4)$$

where ε_c'' is conduction loss, ε_p'' is polarization relaxation loss, ω is angular frequency, σ is dc conductivity, τ is relaxation time and ε_0, ε_s, and ε_∞ are vacuum, static and high-frequency real permittivity, respectively. The conduction loss would be significant in the lower frequency region once the percolating conductive network is formed, and the polarization loss would be negligible compared with the conduction loss. As can be seen from Fig. 6c, there is an apparently linear correlation between ε'' and frequency in the log–log plot for composites containing 55 and 70 wt% Ni/C content, indicating that conduction loss plays a primary role in dielectric loss. The solid line in Fig. 6c represents the calculation results using the conduction loss of eqn (4). The calculation results show good agreement with the experimental data in the lower frequency region (approximately below 6 GHz), while the calculation results obviously deviate from the experimental data in the higher frequency region. It is thought that the leakage currents can no longer keep up with the variation in the high-frequency electromagnetic field and eventually begin to lag, leading to a dielectric response rather than a conduction response to the external altering electromagnetic field.[76] Fig. 6c shows the logarithmic coordinates, and the intercept has a positive correlation with $\ln(\sigma/\varepsilon_0)$, hence, it can be observed that the electrical conductivity of the composites increases with increasing Ni/C content (Fig. 6c). The calculation results (solid lines of the composites containing 55 and 70% Ni/C) indicate the formation of an enhanced percolating conductive network. The conduction loss would be significant with the formation of percolating conductive networks. Conduction loss is beneficial for microwave absorption according to the microwave absorption mechanism (dielectric polarization loss, conduction loss and magnetic loss),[2,3] however, the whole conductive network across the paraffin composites would lead to poor impedance matching, which is harmful to microwave absorption (Fig. S2, ESI†), especially when the absorber has good electrical conductivity.[25] The dielectric loss (dielectric polarization loss and conduction loss) is important to microwave absorbing materials[3,77] and optimal synergistic effects of the polarization loss and conduction loss are necessary for absorption composites.[78–83] When the Ni/C content is too

Fig. 7 Frequency dependence of the RL curves for the paraffin composites with 25 wt% (a) and 30 wt% (b) Ni/C at certain thicknesses.

This journal is © The Royal Society of Chemistry 2018

J. Mater. Chem. C, 2018, **6**, 8812–8822 | **8817**

low, the dielectric loss is not high enough to exhibit good absorption properties (Fig. S3 and S4, ESI†). Therefore, an appropriate Ni/C content should be chosen. That is, the Ni/C content should be near but still below the percolation threshold, hence, there could be enough Ni/C powder for microwave absorption and the leakage current could be suppressed at the same time to allow for a good impedance match.

Based on the analysis above, the paraffin composites containing 25 and 30 wt% Ni/C powder were applied as the absorbing composites and their RL curves are shown in Fig. 7. The RL values of −10 and −20 dB correspond to 90% and 99% attenuation of the incident EM wave.[2–9] For the composites containing 25 wt% Ni/C, the absolute minimum RL value increases with increasing thickness, whereas the absorption bandwidth decreases with increasing thickness, as shown in Fig. 7a. At a thickness of 1.75 mm, the minimum RL value is 21.24 dB, and the maximum absorption bandwidth is 4.4 GHz for RL = −10 dB. When the thickness of the absorbing material is 2 mm, the minimum RL value is 21.2 dB, and the maximum absorption bandwidth is 3.2 GHz for RL= −10 dB. When the Ni/C content increases to 30 wt%, the maximum absorption bandwidth increases to 4.8 GHz for RL = −10 dB at a thinner thickness of 1.5 mm. Relevant investigations into nickel-based nanocomposites are summarized in Table 1. The excellent absorbing properties of the materials produced in this work

indicate that the bio-gel derived strategy is desirable for preparing microwave absorbing materials of thin thickness, light weight and broad absorbing bandwidth.[84–87] More importantly, the bio-gel derived strategy is expected to open the door for the mass synthesis of nanoscale microwave absorbers with porous and multilevel microstructures. The absorbing mechanism is analyzed in the next section.

As shown in Fig. 8a, the real permittivity declines in the frequency range of 2–18 GHz because the dipoles in the composites can no longer keep up with the high-frequency electromagnetic field and eventually begin to lag, resulting in no contribution to the dielectric response. It is a relaxation process of dipoles,[88,89] and there are four different regions for the dielectric response (represented by four colors in Fig. 8). It should be noted that two Debye-like dielectric relaxations are obviously observed in the ε_r' spectra, as shown in Fig. 8a (designated as parts II and III), and the ε_r' displays an obvious decline in these frequency regions (6.5–12 GHz and 12–16.5 GHz) where $\tan\delta$ shows the relaxation peaks at the corresponding frequency (9.2 GHz and 14.8 GHz) in Fig. 8b.[90,91] In addition, as we can see from the curve in Fig. 8b, there should be a loss peak below 6.5 GHz and another above 16.5 GHz (designated as part I and IV), though they are not completely observed in the test frequency region, which is demonstrated by the obvious decrease of ε' in the regions of 2–6.5 GHz and 16.5–18 GHz.

Table 1 Microwave absorption properties of nickel-based materials

| Samples	Mass ratio (%)	Minimum RL value (dB)	RL ≤ −10 dB		Ref.
			d_m (mm)	Frequency range (GHz)	
Ni/C microspheres	75	−28.4	1.8	~12.5–17.4	25
Ni/C core–shell structure	40	−23.4	1.9	~12.8–17.5	26
Ni/C core–shell structure	60	~−38	3	~5–14	27
Ni@C nanosphere	40	~−18	9	~12.2–15.2	28
Ni/C core–shell structure	50	−34	3.5	~7–11	29
Ni/C core–shell structure	55	~−18	3.8	~7.3–10.2	39
Hollow nickel spheres	25	~−26	1.4	~12.5–14.5	22
Ni@C nanoparticles	18.2	~−23	2.5	~11.2–17.1	31
Nickel chains	60	~−25	2	~8.4–10.4	20
Ni/graphene composites	20	~−13	2	~13.5–17.7	32
Ni@C nanorods	60	~−18	1.7	~13–18	33
Ni/C nanocomposites	30	−17.6	1.5	13.2–18	This work
Ni/C nanocomposites	25	−21.2	1.75	13.6–18	This work
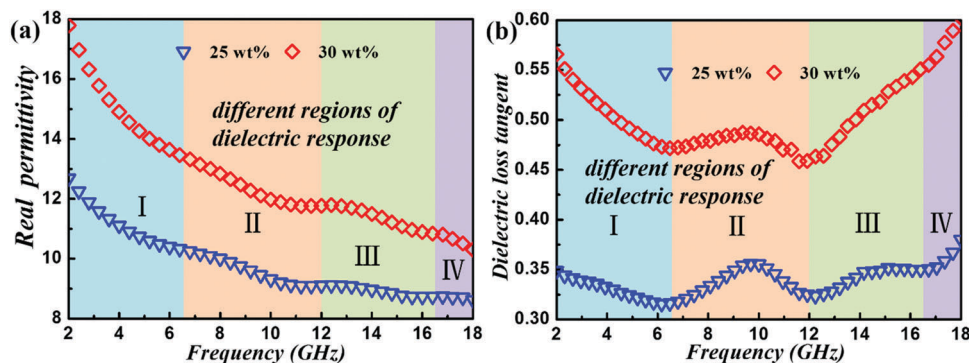
Fig. 8 Real permittivity (a) and dielectric loss tangent ($\tan\delta$) (b) spectra of the paraffin composites containing 25 wt% and 30 wt% Ni/C powder in the 2–18 GHz region. The four colors indicate the different relaxation processes.

As we know, one dielectric relaxation process is always attached to another, so these two regions of dielectric response (below 6.5 GHz and above 16.5 GHz) are parts of dielectric relaxation.[69,71,92] The relaxation behavior is not only attributed to the interfacial polarization due to the significant electrical difference among the nickel particles, carbon sheets and paraffin matrix, but is also attributed to the permanent electric dipoles resulting from defects in the porous amorphous carbon.[25]

Cole–Cole plots were used to investigate the relaxation behavior, as shown in Fig. 9. In an ideal mono-dispersive Debye-type relaxation process, the curve of the experimental data is a semicircle with its centre located on the ε_r' axis in the Cole–Cole plot.[88,89] As shown in Fig. 9, both curves contain four parts, indicating the existence of four different regions of

dielectric response. Two semicircles at 6.5–12 GHz and 12–16.5 GHz and two circular arcs at 2–6.5 GHz and 16.5–18 GHz correspond to parts I–IV in Fig. 8a. However, the curves of the two composites are not perfect semicircles, and the circle centers of the two curves are not located on the ε_r' axis (Fig. 9). This is mainly because the relaxation reported in this work is a multi-relaxation process. That is, when several relaxation processes are added together, each separate relaxation would deviate from ideal Debye-type relaxation.[90,91] The multiple relaxation processes in the Ni/C nanocomposites are related to the Debye dipole in porous amorphous carbon materials and interfacial relaxation on the nickel–carbon interface as well as the Ni/C-paraffin interface, which demonstrates the viewpoint that the construction of multilevel nanostructures can bring more dielectric loss mechanisms.[3] Similar results were also reported by others, in which a multilevel carbon structure played a more dominant role in determining the dielectric loss rather than the isolated magnetic metal.[25–29]

As shown in Fig. S5 (ESI†), the hysteresis loops indicate that the Ni/C powders exhibit magnetic properties due to the existence of nickel particles, which makes it possible to show high-frequency magnetic properties and match with the dielectric properties.[93,94] Fig. 10 shows the complex permeability of the paraffin composites containing 25 and 30 wt% Ni/C powder at 2–18 GHz. The permeability spectra exhibit obvious frequency dispersion at 2–18 GHz, and a large decline of μ' can be seen from 2–8 GHz corresponding to two loss peaks (Fig. 10b), which shows the relaxation behavior of the magnetic domain. Hysteresis loss is negligible in a weak electromagnetic field, and the domain wall resonance loss usually appears under 2 GHz. In addition, leakage current across the whole composite can also be negligible, contributing to good impedance matching, because the Ni/C content is below the percolation threshold and does not form a percolating conductive network in the composites containing 25 and 30 wt% of Ni/C.[95] Therefore, natural ferromagnetic resonance is generally considered as the main magnetic loss mechanism in the 2–18 GHz region.[96,97] The natural resonance frequency shows a linear relationship with the anisotropy field:[98] $2\pi f_r = \gamma H_{eff}$, where f_r is the resonance frequency, γ is the gyromagnetic ratio and H_{eff} is the effective anisotropy field. When the magnetic metal is at the nanoscale, the effective anisotropy field, H_{eff}, can be effectively influenced by particle size, morphology and the anisotropy of
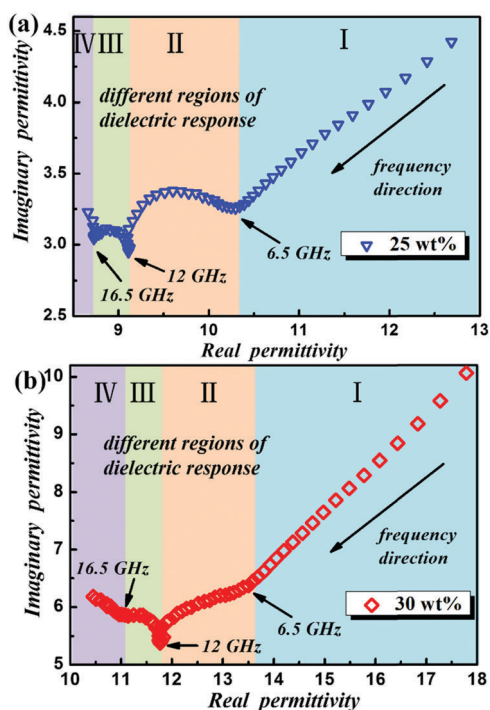

Fig. 9 Cole–Cole plots of the paraffin composites containing 25 wt% (a) and 30 wt% (b) Ni/C powder. The four colors indicate the different relaxation processes.
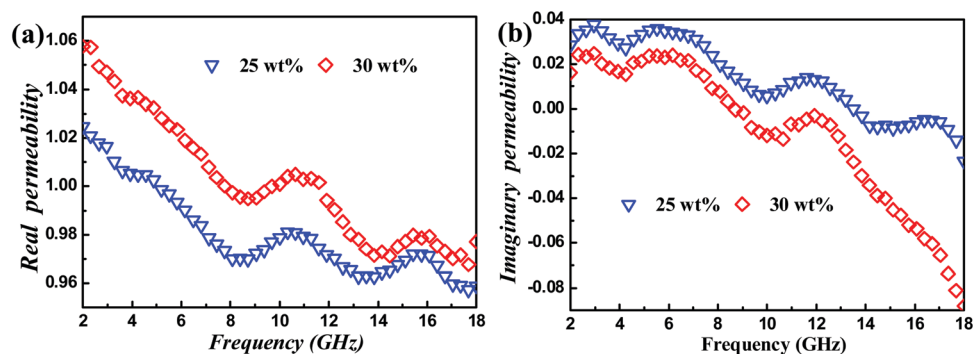

Fig. 10 Real permeability (a) and imaginary permeability (b) of the paraffin composites containing 25% and 30% Ni/C powder in the 2–18 GHz region.

the magnetic domain. The magnetic nanoparticles lead to an increase in H_{eff}, and thus an increase in the natural resonance frequency.[19–22] Therefore, the natural resonances in the 2–18 GHz region may be attributed to the distribution of nickel particle size at the nanoscale (Fig. 10). Similar magnetic behavior has also been observed in some composites containing nanoscale nickel or cobalt particles.[3,4,25–30] Therefore, the magnetic loss is attributed to the ferromagnetic resonance of the nickel particles, which is beneficial for good impedance matching and electromagnetic absorption properties. It is worth noting that the μ'' values are negative in some frequency regions (Fig. 10b), suggesting that the porous Ni/C composites might be used as metamaterials with negative electromagnetic parameters, which usually show unique physical properties different from naturally occurring materials.[79,99] Similar phenomena have also been found in Ni/C microspheres.[25]

4. Conclusion

In this research, we have presented a bio-gel derived strategy to construct novel Ni/C nanocomposites consisting of a porous carbon matrix with embedded nickel nanoparticles. The amorphous carbon prevents the agglomeration of the nickel nanoparticles, which contributes to good impedance matching. According to percolation theory, an appropriate Ni/C content (25 and 30 wt%) was determined in the absorbing coatings to show good impedance matching. As a result, strong reflection loss (RL < −10 dB) was achieved with the advantage of thin thickness (1.75 mm and 1.5 mm), light weight (25 wt% and 30 wt%) and broad bandwidth (13.6–18 GHz and 13.2–18 GHz). The excellent absorbing properties are mainly attributed to the dielectric relaxation loss of the multilevel carbon structure and ferromagnetic resonance of the nickel nanoparticles. This work provides a new design paradigm to determine the optimal content of absorber using percolation theory, and the bio-gel derived strategy paves a possible way for the mass synthesis of nanoabsorbers. Meanwhile, these materials can be used for other applications including environmental remediation,[100] sensing,[101] catalysis,[102] and drug delivery.[103]

Conflicts of interest

There are no conflicts to declare.

Acknowledgements

References

1 F. Shahzad, M. Alhabeb, C. B. Hatter, B. Anasori, H. S. Man, C. M. Koo and Y. Gogotsi, *Science*, 2016, **353**(6304), 1137.

2 M. Han, X. Yin, X. Li, B. Anasori, L. Zhang, L. Cheng and Y. Gogotsi, *ACS Appl. Mater. Interfaces*, 2017, **9**, 20038–20045.

3 D. Ding, P. Xu, R. Qiang, W. Chu, X. Han, X. Li, Y. Wang and Y. Du, *Carbon*, 2017, **111**, 722–732.

4 T. Liu, X. Xie, Y. Pang and S. Kobayashi, *J. Mater. Chem. C*, 2016, **4**(8), 1727–1735.

5 N. Wu, J. Qiao, J. Liu, W. Du, D. Xu and W. Liu, *Adv. Compos. Hybrid Mater.*, 2018, **1**, 149–159.

6 M. Cao, C. Han, X. Wang, M. Zhang, Y. Zhang, J. Shu, H. Yang, X. Fang and J. Yuan, *J. Mater. Chem. C*, 2018, **6**, 4586–4602.

7 M. Cao, X. Wang, W. Cao and J. Yuan, *J. Mater. Chem. C*, 2015, **3**(26), 6589–6599.

8 W. Cao, X. Wang, J. Yuan, W. Wang and M. Cao, *J. Mater. Chem. C*, 2015, **3**(38), 10017–10022.

9 M. Cao, J. Yang, W. Song, D. Zhang, B. Wen, H. Jin, Z. Hou and J. Yuan, *ACS Appl. Mater. Interfaces*, 2012, **4**(12), 6949–6956.

10 (*a*) B. Quan, X. Liang, G. Ji, Y. Zhang, G. Xu and Y. Du, *ACS Appl. Mater. Interfaces*, 2017, **9**(44), 38814–38823; (*b*) B. Quan, X. Liang, G. Ji, J. Ma, P. Ouyang, H. Gong, G. Xu and Y. Du, *ACS Appl. Mater. Interfaces*, 2017, **9**(11), 9964–9974.

11 H. Wu, X. Huang and L. Qian, *Eng. Sci.*, 2018, **2**, 17–25.

12 (*a*) H. Lv, Y. Guo, G. Wu, G. Ji, Y. Zhao and Z. J. Xu, *ACS Appl. Mater. Interfaces*, 2017, **9**(6), 5660–5668; (*b*) L. Lv, J. Liu, H. Liu, C. Liu, Y. Lu, K. Sun, R. Fan, N. Wang, N. Lu, Z. Guo and E. K. Wujcik, *Eng. Sci.*, 2018, **2**, 26–42.

13 X. Jian, B. Wu, Y. Wei, S. Dou, X. Wang, W. He and N. Mahmood, *ACS Appl. Mater. Interfaces*, 2016, **8**(9), 6101.

14 P. Toneguzzo, G. Viau, O. Acher, F. Fiévet-Vincent and F. Fiévet, *Adv. Mater.*, 1998, **10**(13), 1032–1035.

15 L. Qiao, X. Han, B. Gao, J. Wang, F. Wen and F. Li, *J. Appl. Phys.*, 2009, **105**(5), 104325.

16 D. Rousselle, A. Berthault, O. Acher, J. P. Bouchaud and P. G. Zerah, *J. Appl. Phys.*, 1993, **74**(1), 475–479.

17 S. Sugimoto, T. Maeda, D. Book, T. Kagotani, K. Inomata, M. Homma, H. Ota, Y. Houjou and R. Sato, *J. Alloys Compd.*, 2002, **330–332**, 301–306.

18 Y. Li, J. Wang, R. Liu, X. Zhao, X. Wang, X. Zhang and G. Qin, *J. Alloys Compd.*, 2017, **724**, 1023–1029.

19 J. R. Liu, M. Itoh, M. Terada, T. Horikawa and K. Machida, *Appl. Phys. Lett.*, 2007, **91**, 65.

20 C. Wang, X. Han, X. Zhang, S. Hu, T. Zhang, J. Wang, Y. Du, X. Wang and P. Xu, *J. Phys. Chem. C*, 2010, **114**, 3196–3203.

21 C. He, S. Qiu, X. Wang, J. Liu, L. Luan, W. Liu, M. Itoh and K. Machida, *J. Mater. Chem.*, 2012, **22**, 22160–22166.

22 G. Wang, L. Wang, Y. Gan and L. Wei, *Appl. Surf. Sci.*, 2013, **276**, 744–749.

23 G. Wang, X. Peng, L. Yu, G. Wan, S. Lin and Y. Qin, *J. Mater. Chem. A*, 2015, **3**, 2734–2740.

24 X. F. Zhang, H. Huang and X. L. Dong, *J. Phys. Chem. C*, 2013, **117**, 8563–8569.

25 S. Qiu, H. Lyu, J. Liu, Y. Liu, N. Wu and W. Liu, *ACS Appl. Mater. Interfaces*, 2016, **8**, 20258–20266.

26 W. Liu, Q. Shao, G. Ji, X. Liang, Y. Cheng, B. Quan and Y. Du, *Chem. Eng. J.*, 2017, **313**, 734–744.

27 Y. Huang, H. Zhang, G. Zeng, Z. Li, D. Zhang, H. Zhu, R. Xie, L. Zheng and J. Zhu, *J. Alloys Compd.*, 2016, **682**, 138–143.

28 Z. Su, J. Tao, J. Xiang, Y. Zhang, C. Su and F. Wen, *Mater. Res. Bull.*, 2016, **84**, 445–448.

29 N. Wu, X. Liu, C. Zhao, C. Cui and A. Xia, *J. Alloys Compd.*, 2016, **656**, 628–634.

30 N. Wu, H. Lv, J. Liu, Y. Liu, S. Wang and W. Liu, *Phys. Chem. Chem. Phys.*, 2016, **18**, 31542–31550.

31 N. Li, M. Cao and C. Hu, *J. Mater. Chem.*, 2012, **22**, 18426–18432.

32 Y. Cao, Q. Su, R. Che, G. Du and B. Xu, *Synth. Met.*, 2012, **162**, 968–973.

33 Y. Zhang, X. Zhang, B. Quan, G. Ji, X. Liang, W. Liu and Y. Du, *Nanotechnology*, 2017, **28**, 115704.

34 N. Wu, X. Liu and S. W. Or, *AIP Adv.*, 2016, **6**, 056206.

35 T. Wu, Y. Liu, X. Zeng, T. Cui, Y. Zhao, Y. Li and G. Tong, *ACS Appl. Mater. Interfaces*, 2016, **8**, 7370–7380.

36 Q. Liu, Q. Cao, H. Bi, C. Liang, K. Yuan, W. She, Y. Yang and R. Che, *Adv. Mater.*, 2016, **28**, 486–490.

37 X. Liu, S. Wing Or, C. Ming Leung and S. Ho, *J. Appl. Phys.*, 2014, **115**, 053115.

38 (a) H. Meng, X. Zhao, L. Yu, Y. Jia, H. Liu, X. Lv, C. Gong and J. Zhou, *J. Alloys Compd.*, 2015, **644**, 236–241; (b) F. Liu, Z. Xu, Z. Wang, M. Dong, J. Deng, Q. Yao, H. Zhou, Y. Ma, J. Zhang, N. Wang and Z. Guo, *J. Alloys Compd.*, 2018, **756**, 26–32.

39 H. Wang, H. Guo, Y. Dai, D. Geng, Z. Han, D. Li, T. Yang, S. Ma, W. Liu and Z. Zhang, *Appl. Phys. Lett.*, 2012, **101**, 083116.

40 F. Dang, Y. Oaki, T. Kokubu, E. Hosono, H. Zhou and H. Imai, *Chem. – Asian J.*, 2013, **8**, 760–764.

41 F. Dang, T. Hoshino, Y. Oaki, E. Hosono, H. Zhou and H. Imai, *Nanoscale*, 2013, **5**, 2352–2357.

42 C. Hou, Y. Oaki, E. Hosono, H. Lin, H. Imai, Y. Fan and F. Dang, *Mater. Des.*, 2016, **109**, 718–725.

43 W. Song, X. Guan, L. Fan, Y. Zhao, W. Cao, C. Wang and M. Cao, *Carbon*, 2016, **100**, 109–117.

44 Y. Pan, G. Wang, L. Liu, L. Guo and S. Yu, *Nano Res.*, 2017, **10**(1), 284–294.

45 W. Song, L. Fan, Z. Hou, K. Zhang, Y. Ma and M. Cao, *J. Mater. Chem. C*, 2017, **5**(9), 2432–2441.

46 K. Gong, Q. Hu, L. Yao, M. Li, D. Sun, Q. Shao, B. Qiu and Z. Guo, *ACS Sustainable Chem. Eng.*, 2018, **6**, 7283–7291.

47 M. Han, X. Yin, S. Ren, W. Duan, L. Zhang and L. Cheng, *RSC Adv.*, 2016, **6**(8), 6467–6474.

48 (a) L. Zhang, W. Yu, C. Han, J. Guo, Q. Zhang, H. Xie, Q. Shao, Z. Sun and Z. Guo, *J. Electrochem. Soc.*, 2017, **164**, H651–H656; (b) L. Zhang, M. Qin, W. Yu, Q. Zhang, H. Xie, Z. Sun, Q. Shao, X. Guo, L. Hao, Y. Zheng and Z. Guo, *J. Electrochem. Soc.*, 2017, **164**, H1086–H1090.

49 Q. Luo, H. Ma, F. Hao, Q. Hou, J. Ren, L. Wu, Z. Yao, Y. Zhou, N. Wang, K. Jiang, H. Lin and Z. Guo, *Adv. Funct. Mater.*, 2017, **27**(42), 1703068.

50 J. Tian, Q. Shao, X. Dong, J. Zheng, D. Pan, X. Zhang, H. Cao, L. Hao., J. Liu and Z. Guo, *Electrochim. Acta*, 2018, **261**, 236–245.

51 M. Chen, B. Yang, J. Zhu, H. Liu, X. Zhang, X. Zheng and Q. Liu, *Mater. Sci. Eng. C*, 2018, **90**, 610–620.

52 A. Ferrari, B. Kleinsorge, N. Morrison, A. Hart, V. Stolojan and J. Robertson, *J. Appl. Phys.*, 1999, **85**(10), 7191–7197.

53 A. C. Ferrari and J. Robertson, *Phys. Rev. B: Condens. Matter Mater. Phys.*, 2000, **61**(20), 14095.

54 Y. Li, B. Zhou, G. Zheng, X. Liu, T. Li, C. Yan, C. Cheng, K. Dai, C. Liu, C. Shen and Z. Guo, *J. Mater. Chem. C*, 2018, **6**, 2258–2269.

55 H. Liu, M. Dong, W. Huang, J. Gao, K. Dai, J. Guo, G. Zheng, C. Liu, C. Shen and Z. Guo, *J. Mater. Chem. C*, 2017, **5**, 73–83.

56 C. Hu, Z. Li, Y. Wang, J. Gao, K. Dai, G. Zheng, C. Liu, C. Shen, H. Song and Z. Guo, *J. Mater. Chem. C*, 2017, **5**, 2318–2328.

57 S. Ge, X. Yang, Q. Shao, Q. Liu, T. Wang, L. Wang and X. Wang, *J. Solid State Chem.*, 2013, **200**, 136–142.

58 X. Guan, G. Zheng, K. Dai, C. Liu, X. Yan, C. Shen and Z. Guo, *ACS Appl. Mater. Interfaces*, 2016, **8**, 14150–14159.

59 T. Wu, Q. Shao, S. Ge, L. Bao and Q. Liu, *RSC Adv.*, 2016, **6**(63), 58020–58027.

60 P. Xie, Z. Zhang, K. Liu, L. Qian, F. Dang, Y. Liu, R. Fan, X. Wang and S. Dou, *Carbon*, 2017, **125**, 1–8.

61 K. Sun, R. Fan, X. Zhang, Z. Zhang, Z. Shi, N. Wang, P. Xie, Z. Wang, G. Fan, H. Liu, C. Liu, T. Li, C. Yan and Z. Guo, *J. Mater. Chem. C*, 2018, **6**, 2925–2943.

62 C. Cheng, R. Fan, Z. Wang, Q. Shao, X. Guo, P. Xie, Y. Yin, Y. Zhang, L. An and Y. Lei, *Carbon*, 2017, **125**, 103–112.

63 Y. Guo, G. Xu, X. Yang, K. Ruan, T. Ma, Q. Zhang, J. Gu, Y. Wu, H. Liu and Z. Guo, *J. Mater. Chem. C*, 2018, **6**, 3004–3015.

64 (a) M. Zhao, L. Meng, L. Ma, L. Ma, X. Yang, Y. Huang, J. E. Ryu, A. Shankar, T. Li, C. Yan and Z. Guo, *Compos. Sci. Technol.*, 2018, **154**, 28–36; (b) Z. Wu, H. Cui, L. Chen, D. Jiang, L. Weng, Y. Ma, X. Li, X. Zhang, H. Liu, N. Wang, J. Zhang, Y. Ma, M. Zhang, Y. Huang and Z. Guo, *Compos. Sci. Technol.*, 2018, **164**, 195–203.

65 M. Han, X. Yin, H. Wu, Z. Hou, C. Song, X. Li, L. Zhang and L. Cheng, *ACS Appl. Mater. Interfaces*, 2016, **8**(32), 21011–21019.

66 W. Sun, A. Du, Y. Feng, J. Shen, S. Huang, J. Tang and B. Zhou, *ACS Nano*, 2016, **10**(10), 9123–9128.

67 C. F. Martín, E. Stöckel, R. Clowes, D. J. Adams, A. I. Cooper, J. J. Pis, F. Rubiera and C. Pevida, *J. Mater. Chem.*, 2011, **21**(14), 5475–5483.

68 N. Yousefi, X. Sun, X. Lin, X. Shen, J. Jia, B. Zhang, B. Tang, M. Chan and J. K. Kim, *Adv. Mater.*, 2014, **26**(31), 5480–5487.

69 Z. M. Dang, M. S. Zheng and J. W. Zha, *Small*, 2016, **12**(13), 1688–1701.

70 S. Luo, Y. Shen, S. Yu, Y. Wan, W. Liao, R. Sun and C. Wong, *Energy Environ. Sci.*, 2017, **10**(1), 137–144.

71 P. Xie, K. Sun, Z. Wang, Y. Liu, R. Fan, Z. Zhang and G. Schumacher, *J. Alloys Compd.*, 2017, **725**, 1259–1263.

72 P. Xie, Z. Wang, K. Sun, C. Cheng, Y. Liu and R. Fan, *Appl. Phys. Lett.*, 2017, **111**(11), 112903.

This journal is © The Royal Society of Chemistry 2018

J. Mater. Chem. C, 2018, **6**, 8812–8822 | 8821

73 C. W. Nan, Y. Shen and J. Ma, *Annu. Rev. Mater. Res.*, 2010, **40**(1), 131–151.

74 Z. M. Dang, Y. H. Lin and C. W. Nan, *Adv. Mater.*, 2003, **15**(19), 1625–1629.

75 K. Sun, P. Xie, Z. Wang, T. Su, Q. Shao, J. Ryu, X. Zhang, J. Guo, A. Shankar, J. Li, R. Fan, D. Cao and Z. Guo, *Polymer*, 2017, **125**, 50–57.

76 W. J. Padilla, D. N. Basov and D. R. Smith, *Mater. Today*, 2006, **9**(7), 28–35.

77 C. Cheng, R. Fan, Y. Ren, T. Ding, L. Qian, J. Guo, X. Li, L. An, Y. Lei, Y. Yin and Z. Guo, *Nanoscale*, 2017, **9**(18), 5779–5787.

78 B. Wen, M. Cao, M. Lu, W. Cao, H. Shi, J. Liu, X. Wang, H. Jin, X. Fang, W. Wang and J. Yuan, *Adv. Mater.*, 2014, **26**(21), 3484–3489.

79 X. Wang, T. Ma, J. Shu and M. Cao, *Chem. Eng. J.*, 2018, **332**, 321–330.

80 Y. Zhang, X. Wang and M. Cao, *Nano Res.*, 2018, **11**(3), 1426–1436.

81 M. Cao, W. Song, Z. Hou, B. Wen and J. Yuan, *Carbon*, 2010, **48**(3), 788–796.

82 X. Shi, M. Cao, J. Yuan and X. Fang, *Appl. Phys. Lett.*, 2009, **95**(16), 163108.

83 B. Wen, M. Cao, Z. Hou, W. Song, L. Zhang, M. Lu, H. Jin, X. Fang, W. Wang and J. Yuan, *Carbon*, 2013, **65**, 124–139.

84 X. Zhang, G. Ji, W. Liu, B. Quan, X. Liang, C. Shang, Y. Cheng and Y. Du, *Nanoscale*, 2015, **7**, 12932–12942.

85 H. Lv, X. Liang, G. Ji, H. Zhang and Y. Du, *ACS Appl. Mater. Interfaces*, 2015, **7**(18), 9776–9783.

86 X. Zhang, G. Ji, W. Liu, X. Zhang, Q. Gao, Y. Li and Y. Du, *J. Mater. Chem. C*, 2016, **4**(9), 1860–1870.

87 H. Lv, Z. Yang, P. L. Wang, G. Ji, J. Song, L. Zheng, H. Zeng and Z. J. Xu, *Adv. Mater.*, 2018, **30**(15), 1706343.

88 J. Chen and Z. Liu, *Dielectric physics*, China Machine Press, 1982, pp. 170–178.

89 J. Ma, X. Wang, W. Cao, C. Han, H. Yang, J. Yuan and M. Cao, *Chem. Eng. J.*, 2018, **339**, 487–498.

90 H. Wu, Y. Zhang, R. Yin, W. Zhao, X. Li and L. Qian, *Adv. Compos. Hybrid Mater.*, 2017, **1**, 168–176.

91 P. Xie, Z. Wang, Z. Zhang, R. Fan, C. Cheng, H. Liu, Y. Liu, T. Li, C. Yan, N. Wang and Z. Guo, *J. Mater. Chem. C*, 2018, **6**, 5239–5249.

92 L. Y. Zhang and X. Yao, *Dielectric Physics*, Xi'an Jiaotong University Press, Xi'an, 1991, p. 175.

93 W. Deng, T. Kang, H. Liu, J. Zhang, N. Wang, N. Lu, Y. Ma, A. Umar and Z. Guo, *Sci. Adv. Mater.*, 2018, **10**, 937–949.

94 X. Zhu, W. Chen, K. Wu, H. Li, M. Fu, Q. Liu and X. Zhang, *New J. Chem.*, 2018, **42**, 1501–1509.

95 T. Tsutaoka, H. Massango, T. Kasagi, S. Yamamoto and K. Hatakeyama, *Appl. Phys. Lett.*, 2016, **108**(19), 191904.

96 B. Lu, X. Dong, H. Huang, X. Zhang, X. Zhu, J. Lei and J. Sun, *J. Magn. Magn. Mater.*, 2008, **320**(6), 1106–1111.

97 X. Zhang, X. Dong, H. Huang, Y. Liu, W. Wang, X. Zhu, B. Lv, J. Lei and C. Lee, *Appl. Phys. Lett.*, 2006, **89**, 053115.

98 C. Kittel, *Phys. Rev.*, 1948, **73**, 155.

99 P. Xie, W. Sun, Y. Liu, A. Du, Z. Zhang, G. Wu and R. Fan, *Carbon*, 2018, **129**, 598–606.

100 (*a*) J. Huang, Y. Cao, Q. Shao, X. Peng and Z. Guo, *Ind. Eng. Chem. Res.*, 2017, **56**, 10689–10701; (*b*) Y. Wang, P. Zhou, S. Luo, S. Guo, J. Lin, Q. Shao, X. Guo, Z. Liu, J. Shen, B. Wang and Z. Guo, *Adv. Polym. Technol.*, 2018, DOI: 10.1002/adv.21969; (*c*) Y. Zhang, M. Zhao, J. Zhang, Q. Shao, J. Li, H. Li, B. Lin, M. Yu, S. Chen and Z. Guo, *J. Polym. Res.*, 2018, **25**, 130; (*d*) Z. Hu, Q. Shao, Y. Huang, L. Yu, D. Zhang, X. Xu, J. Lin, H. Liu and Z. Guo, *Nanotechnology*, 2018, **29**, 185602; (*e*) K. Gong, Q. Hu, Y. Xiao, X. Cheng, H. Liu, N. Wang, B. Qiu and Z. Guo, *J. Mater. Chem. A*, 2018, **6**, 11119; (*f*) J. Huang, Y. Li, Y. Cao, F. Peng, Y. Cao, Q. Shao, H. Liu and Z. Guo, *J. Mater. Chem. A*, 2018, DOI: 10.1039/C8TA02861C; (*g*) H. L. Shindume, Z. Zhao, N. Wang, H. Liu, A. Umar, J. Zhang, T. Wu and Z. Guo, *J. Nanosci. Nanotechnol.*, 2018, DOI: 10.1166/jnn.2018.15745; (*h*) J. Zhao, S. Ge, L. Liu, Q. Shao, X. Mai, C. X. Zhao, L. Hao, T. Wu, Z. Yu and Z. Guo, *Ind. Eng. Chem. Res.*, 2018, **57**, 231–241; (*i*) S. Ge, L. Bao and Q. Liu, *RSC Adv.*, 2016, **6**, 58020–58027.

101 (*a*) H. Gu, H. Zhang, J. Lin, Q. Shao, D. P. Young, L. Sun, T. D. Shen and Z. Guo, *Polymer*, 2018, **143**, 324–330; (*b*) L. Gao, L. Zhang, X. Lyu, G. Lu and Q. Liu, *Eng. Sci.*, 2018, **1**, 69–77; (*c*) H. Liu, W. Huang and X. Yang, *et al.*, *J. Mater. Chem. C*, 2016, **4**, 4459–4469.

102 (*a*) P. Zhou, S. Wang, C. Tao, X. Guo, L. Hao, Q. Shao, L. Liu, Y. Wang, W. Chu, B. Wang, S. Luo and Z. Guo, *Adv. Polym. Technol.*, 2018, DOI: 10.1002/adv.21908; (*b*) B. Song, T. Wang, H. Sun, Q. Shao, J. Zhao, K. Song, L. Hao, L. Wang and Z. Guo, *Dalton Trans.*, 2017, **46**, 15769–15777; (*c*) C. Lin, H. Hu, C. Cheng, K. Sun, X. Guo, Q. Shao, J. Li, N. Wang and Z. Guo, *Electrochim. Acta*, 2018, **260**, 65–72; (*d*) Q. Hou, J. Ren, H. Chen, P. Yang, Q. Shao, M. Zhao, X. Zhao, H. He, N. Wang, Q. Luo and Z. Guo, *ChemElectroChem*, 2018, **5**, 726–731.

103 Z. Hu, D. Zhang, L. Yu and Y. Huang, *J. Mater. Chem. B*, 2018, **6**, 518–526.

8822 | *J. Mater. Chem. C*, 2018, **6**, 8812–8822

This journal is © The Royal Society of Chemistry 2018